



## Recent Results from CDF

Sally Seidel  
New Mexico Center for Particle Physics  
University of New Mexico  
Albuquerque, NM, 87131, USA

*for the CDF Collaboration*

### Abstract

During the past year, the CDF Experiment has reported on a variety of results concerning QCD and electroweak studies, studies of the top quark, and searches for new phenomena. A sample of these results is presented here.

## 1 Introduction

CDF, a multi-purpose detector for studying proton-antiproton collisions at center-of-mass energy 1.8 TeV at the Fermilab Tevatron, has reported on over 20 topics since the previous meeting in this series. This paper summarizes some of those results. Details about the CDF detector may be found in Reference [1].

## 2 QCD Studies Including Those on $B$ Meson Systems

### 2.1 $b - \bar{b}$ Rapidity Correlations

At leading order in QCD,  $b$  pairs are produced through several channels: via  $q - \bar{q}$  annihilation through the  $s$ -channel, leading to rapidity  $y$  correlation<sup>1</sup> of the form  $d\sigma/dt \sim (\cosh\Delta y)^{-2}$  at large  $\Delta y \equiv y_b - y_{\bar{b}}$ , and via gluon fusion, including  $t$ -channel exchange, leading to correlation  $d\sigma/dt \sim (\cosh\Delta y)^{-1}$ . These distributions are expected to be broadened at next-to-leading order (NLO) and affected somewhat by choice of parton distribution function (PDF). The shape of the  $y$  distribution is interesting because it probes the gluon distribution of the proton at high  $x$  for a range from  $x_-$  to  $x_+$  given, for transverse momentum  $p_T$ , by  $x_{\pm} = M_T[e^{\pm y_b} + e^{\pm y_{\bar{b}}}] / \sqrt{s}$ , where  $M_T = \sqrt{m_b^2 + \langle p_T \rangle^2}$  and  $\langle p_T \rangle = (p_T^b + p_T^{\bar{b}})/2$ . Measuring the ratio

$$R \equiv \frac{\sigma(p\bar{p} \rightarrow b_1 b_2 X; 2.0 < |y_{b_1}| < 2.6)}{\sigma(p\bar{p} \rightarrow b_1 b_2 X; |y_{b_1}| < 0.6)}$$

tests QCD at NLO and tests the gluon distribution directly at high  $x$ . This analysis [2] uses events from the muon triggers and identifies  $b\bar{b}$  events in which one  $b$  decays through  $b \rightarrow \mu + \text{jet}$  and the other is identified by secondary vertex reconstruction. The inferred angle between the  $b$ 's is required to be greater than  $60^\circ$  to remove gluon splitting events, which require model-dependent acceptance information. Corrections are made for efficiency, acceptance, and backgrounds including  $c\bar{c}$  production, heavy quarks accompanied by fake muons, events with two fakes, and  $Z^0 \rightarrow b\bar{b}$  events. Backgrounds are distinguished by their transverse momentum  $p_T$  relative to the  $\mu^\pm$  axis (" $p_T^{\text{el}}$ ") and the secondary vertex's "pseudo- $ct$ ," which is related to transverse proper decay length  $L_{xy}$  by pseudo- $ct = L_{xy}M/p_T$ . ( $M$  and  $p_T$  are computed under the assumption that tracks are from pions.) Two classes of events are identified: (1) those with one  $b$  central, the other forward, and (2) those with both  $b$ 's central. The ratio

$$R = \frac{N_{b\bar{b}}^{\text{forward}} / \epsilon_{\text{forward}}}{N_{b\bar{b}}^{\text{central}} / \epsilon_{\text{central}}}$$

is formed, where  $N$  is the number of events observed in the forward or central portion of the detector and  $\epsilon$  is the corresponding efficiency in that region. Figure 1 shows the result for 77 pb<sup>-1</sup>:  $R = 0.361 \pm 0.033^{+0.015}_{-0.031}$ , in good agreement with the theoretical prediction at NLO,  $0.338^{+0.014}_{-0.097}$ , using MRSA' PDF's.

<sup>1</sup>E.L. Berger, Phys. Rev. D **37**, 1810 (1988).

The theoretical error is associated with the scale factor. This is the first direct measurement of the predicted strong  $b\bar{b}$  correlation. Figure 2 shows that the best agreement between data and theory is obtained for the MRSR2 PDF.

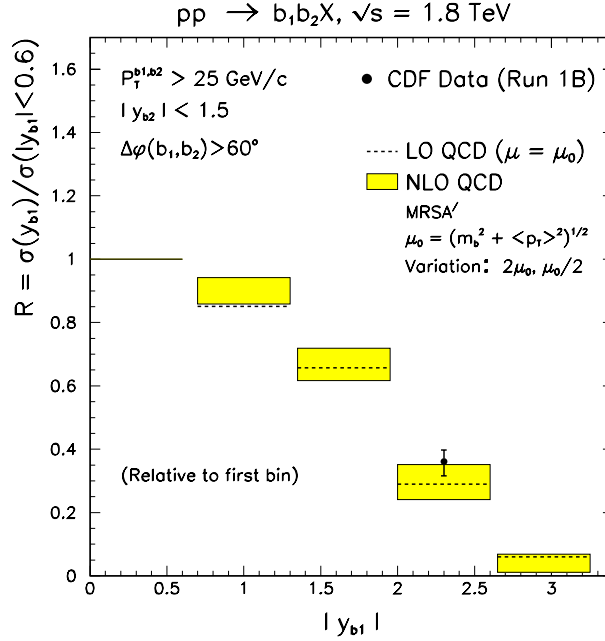


Figure 1: The normalized rapidity distribution of the trigger  $b$  quark. Filled boxes are the theoretical prediction in each bin, taking into account variations in the scale. The dashed line is the leading order prediction, and the experimental measurement is indicated by the point with an error bar.

## 2.2 $b$ Quark Fragmentation Fractions

We define the probabilities  $f_i$  for fragmentation of a  $\bar{b}$  quark to a hadron containing quark type  $i$  such that  $f_u$ ,  $f_d$ ,  $f_s$ , and  $f_{\text{baryon}}$  imply final states containing a  $B^+$ ,  $B^0$ ,  $B_s^0$ , and  $\bar{\Lambda}_b^0$ , respectively. These probabilities include contributions from production of heavier  $B$  hadrons that decay to these final states. This study [3] examines the flavor dependence of the (non-perturbative) fragmentation process. Events from electron triggers are examined, and the following  $B$  decays<sup>2</sup> are reconstructed:

$$\begin{aligned}
 B^+ &\rightarrow \bar{D}^0 e^+ \nu_e X; \bar{D}^0 \rightarrow K^+ \pi^- \\
 B^0 &\rightarrow D^{*-} e^+ \nu_e X; D^{*-} \rightarrow \bar{D}^0 \pi^-; \bar{D}^0 \rightarrow K^+ \pi^- \\
 B^0 &\rightarrow D^- e^+ \nu_e X; D^- \rightarrow K^+ \pi^- \pi^- \\
 B_s^0 &\rightarrow D_s^- e^+ \nu_e X; D_s^- \rightarrow \phi \pi^-; \phi \rightarrow K^+ K^- \\
 \bar{\Lambda}_b^0 &\rightarrow \Lambda_c^- e^+ \nu_e X; \Lambda_c^- \rightarrow \bar{p} K^+ \pi^-.
 \end{aligned} \tag{1}$$

Fits are performed to separate signal and background; the feeddown contribution is removed, and the signal is extracted. Systematic errors include signal reflections and uncertainties associated with assumed signal and background shape parameterizations. The five observed yields are examined for  $107 \text{ pb}^{-1}$  of data in three ratios by using a combined  $\chi^2$  function. Under the assumption that  $f_d/f_u = 1$ , we find that  $f_s/(f_u + f_d) = 0.213 \pm 0.068$  and  $f_{\text{baryon}}/(f_u + f_d) = 0.118 \pm 0.042$ . Under the assumption that  $f_u + f_d + f_s + f_{\text{baryon}} = 1$ ,  $f_u = f_d = 0.375 \pm 0.023$ ,  $f_s = 0.160 \pm 0.044$ , and  $f_{\text{baryon}} = 0.090 \pm 0.029$ . Relaxing the isospin symmetry requirement yields  $f_u/f_d = 0.84 \pm 0.16$ . The  $f_s$  value is two standard deviations above the world average, while  $f_{\text{baryon}}$  is in good agreement with measurements at LEP.

<sup>2</sup>Unless otherwise noted, decay channels imply their charge conjugates as well.

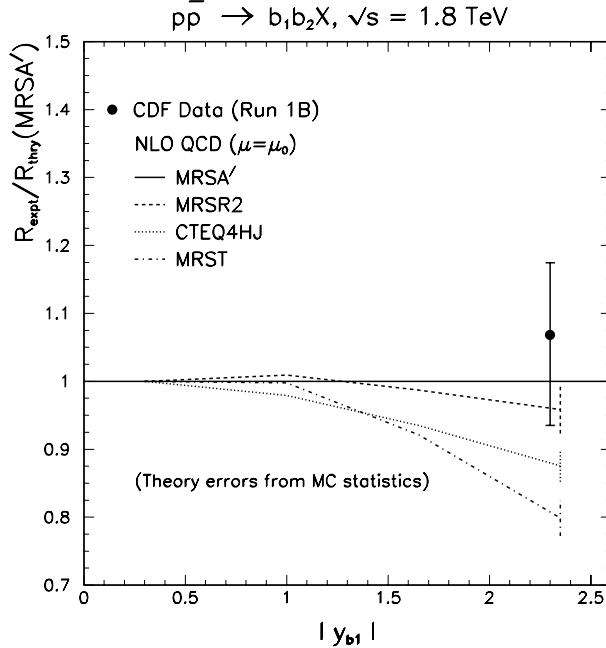


Figure 2: Comparison of the ratio  $R$ , as defined in the text, between data and theory using MRSA' PDF's. Theoretical curves for MRSR2, CTEQ4HJ, and MRST are divided by the MRSA' curve and normalized to unity in the first bin. Theoretical error bars are the statistical uncertainty from Monte Carlo integration, while the data error combines statistical and systematic uncertainties.

### 2.3 $J/\psi$ and $\psi(2S)$ Polarization

CDF has previously reported cross section measurements<sup>3</sup> of the  $J/\psi$  and  $\psi(2S)$  that were fifty times lower than predictions from the Color Singlet Model.<sup>4</sup> The Non-relativistic QCD (NRQCD) factorization formalism<sup>5</sup> may explain the difference. This study [4] examines the prediction by NRQCD that directly produced  $\psi$ 's have polarization proportional to  $p_T$  due to the dominance of gluon fragmentation in the production process. Events from the dimuon ( $\psi \rightarrow \mu^+ \mu^-$ ) trigger are examined. Their reconstructed proper decay length is used where possible to separate  $b$ -produced  $\psi$ 's from prompt ones. We measure

$$I \equiv 3(1 + \alpha \cos^2 \theta^*) / 2(\alpha + 3),$$

where  $\theta^*$  is the angle between the  $\mu^+$  direction in the  $\psi$  rest frame and the  $\psi$  direction in the laboratory frame, and  $\alpha$  equal to +1, 0, or -1 indicates fully transverse polarization, zero polarization, or fully longitudinal polarization, respectively. The value of  $\alpha$  is extracted by comparing measurements to template distributions for events simulated with effects of detector acceptance and reconstruction efficiency included. The fit is made simultaneously for events classified as prompt,  $b$ -produced, and untagged, in 7 bins for  $J/\psi$  and 3 bins for  $\psi(2S)$ . Systematic uncertainties result from trigger inefficiencies, accuracy of fitted decay fractions, and the  $p_T$  spectra used in the templates. Figures 3, 4, and 5 show the result for  $110 \text{ pb}^{-1}$ : no evidence was found for an increase in polarization as a function of  $p_T$  for  $p_T \geq 12 \text{ GeV}/c$ , in contradiction to expectations of the NRQCD model.

<sup>3</sup>F. Abe *et al.*, Phys. Rev. Lett. **79**, 572 (1997); F. Abe *et al.*, Phys. Rev. Lett. **79**, 578 (1997).

<sup>4</sup>M. Cacciari and M. Greco, Phys. Rev. Lett. **73**, 1586 (1994); E. Braaten *et al.*, Phys. Lett. B **333**, 548 (1994); D.P. Roy and K. Sridhar, Phys. Lett. B **339**, 141 (1994).

<sup>5</sup>G. Bodwin, E. Braaten, and G. Lepage, Phys. Rev. D **51**, 1125 (1995); E. Braaten and S. Fleming, Phys. Rev. Lett. **74**, 3327 (1995); P. Cho and M. Wise, Phys. Lett. B **346**, 129 (1995); M. Cacciari *et al.*, Phys. Lett. B **356**, 553 (1995); E. Braaten and Y. Chen, Phys. Rev. D **54**, 3216 (1996); P. Cho and A.K. Leibovich, Phys. Rev. D **53**, 150 (1996); P. Cho and A.K. Leibovich, Phys. Rev. D **53**, 6203 (1996).

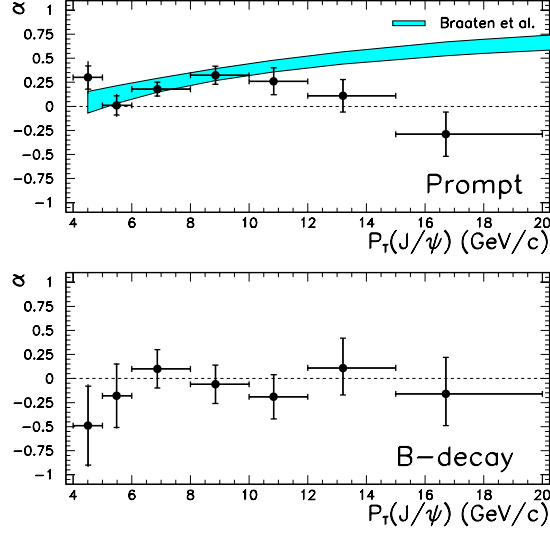


Figure 3: The fitted polarization of  $J/\psi$  mesons from prompt production and  $B$ -hadron decay, in seven  $p_T$  bins, for  $|y^{J/\psi}| < 0.6$ . Full error bars denote statistical and systematic uncertainties added in quadrature; ticks denote statistical errors alone. The shaded band shows a NRQCD factorization prediction which includes the contribution from  $\chi_c$  and  $\psi(2S)$  decays.

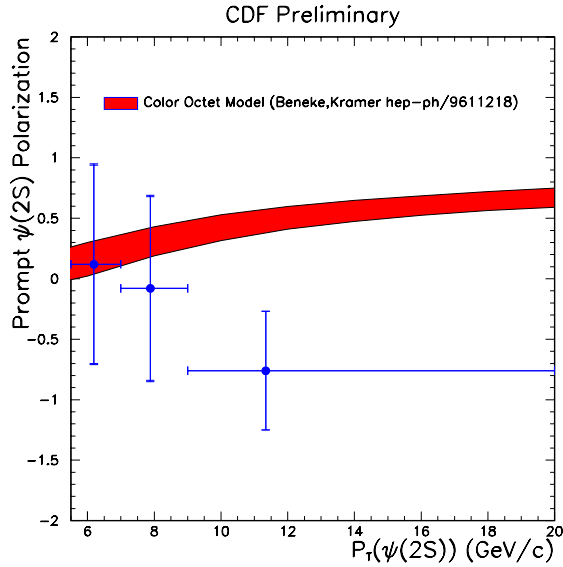


Figure 4: The fitted polarization of  $\psi(2S)$  mesons from prompt production, in three  $p_T$  bins, for  $|y^{J/\psi}| < 0.6$ . Error bars denote statistical and systematic uncertainties added in quadrature. One NRQCD prediction is shown.

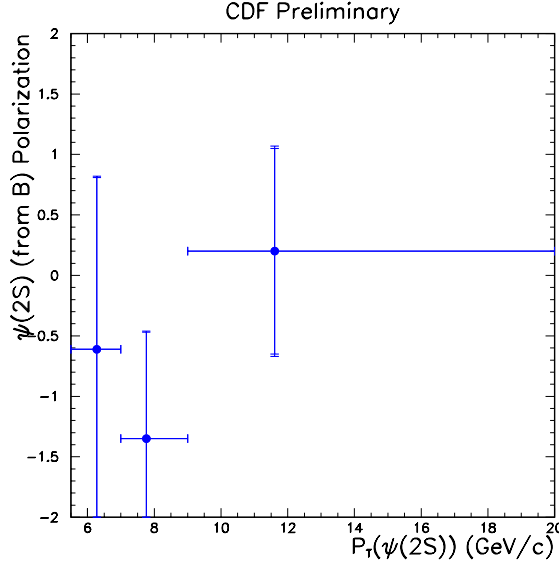


Figure 5: The fitted polarization of  $\psi(2S)$  mesons from production by  $B$  decay, in three  $p_T$  bins, for  $|y^{J/\psi}| < 0.6$ . Error bars denote statistical and systematic uncertainties added in quadrature.

## 2.4 Production of $\Upsilon(1S)$ Mesons from $\chi_b$ Decays

NRQCD factorizes the quarkonium production process into short-distance cross sections (to produce the  $q$  and  $\bar{q}$ ) and long-distance matrix elements to describe their binding into quarkonium. The matrix elements must be determined from data. The ability of NRQCD to explain differences between the Color Singlet Model and CDF measurements of charmonium cross sections motivates this study of  $\Upsilon$  production. Events [5] with dimuons originating at the primary vertex are filtered to select the process  $p\bar{p} \rightarrow \chi_b X$ ;  $\chi_b \rightarrow \Upsilon(1S)\gamma$ ;  $\Upsilon(1S) \rightarrow \mu^+\mu^-$ . To maintain good reconstruction efficiency, the  $p_T$  of the  $\mu\mu$  pair is required to be greater than 8 GeV/c, and the pseudorapidity  $\eta$  of the pair must be central. The reconstructed  $\mu\mu$  invariant mass is required to be consistent with the  $\Upsilon(1S)$  mass (we use the range 9.3–9.6 GeV/c<sup>2</sup>), then the pair is combined with isolated photons within 90° of it. We histogram  $\Delta M \equiv M(\mu\mu\gamma) - M(\mu\mu)$ , estimate background from photons using simulation, and fit the data to two Gaussians (to represent the  $\chi_b(1P)$  and  $\chi_b(2P)$ ) plus background. The result is shown in Figure 6. After correcting for acceptance and efficiency losses and estimating contributions from  $\Upsilon(2S)$ ,  $\Upsilon(3S)$ , and  $\chi_b(3P)$ , we extract the following signals from data of luminosity 90 pb<sup>-1</sup>. The percentage of  $\Upsilon(1S)$  with  $p_T > 8$  GeV/c<sup>2</sup> produced by  $\chi_b(1P)$  is  $(27.1 \pm 6.9 \pm 4.4)\%$ . The percentage produced by  $\chi_b(2P)$  is  $(10.5 \pm 4.4 \pm 1.4)\%$ . The CSM predictions for these percentages are 41% and 13%, respectively. The fraction of  $\Upsilon(1S)$  mesons that are directly produced is found to be  $(50.9 \pm 8.2 \pm 9.0)\%$ .

## 2.5 Orbitaly Excited $B$ Mesons, $B^{**}$

The name  $B^{**}$  refers to any of the four  $L = 1$  states shown in Figure 7. Measurements of these states, which have not been fully resolved, provide a test of Heavy Quark Effective Theory. We consider [6] the following decay sequence:  $B^{**} \rightarrow B^*\pi + B\pi$ ;  $B^* \rightarrow B\gamma$ ;  $B \rightarrow D\ell\nu$ ;  $D \rightarrow K + \text{pions}$ . The lepton from the  $B \rightarrow D\ell\nu$  decay provides the trigger.  $D$  and  $B$  secondary vertices are reconstructed by impact parameter. The  $K$  and  $\ell$  are required to be correlated in sign. After a selection on the meson masses, the remaining  $B$ 's are combined with all prompt tracks; the result is required to originate at the primary vertex and have high  $p_T$ . The measured momentum of the decay products is corrected by an average multiplicative factor to account for the neutrino; the (soft) photon information is lost. We histogram the variable  $Q \equiv M(B\pi) - M(B) - M(\pi)$  and subtract background associated with  $B$ 's from  $b$  hadronization and  $B$  oscillations, fake  $B$ 's, the underlying event, and multiple interactions. The  $Q$  distribution is

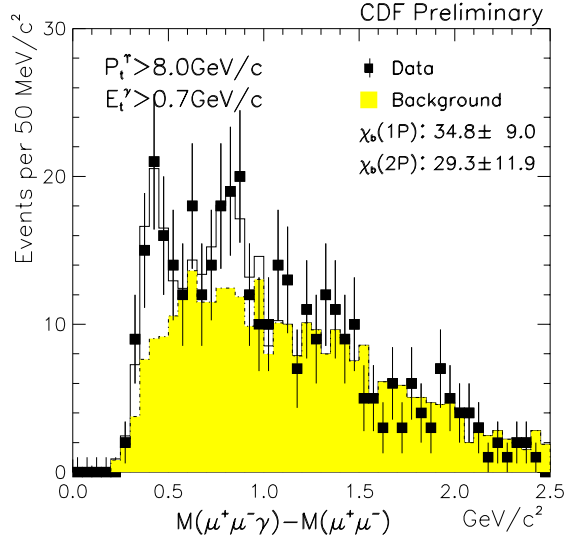


Figure 6: The mass difference distribution,  $\Delta M$ . The points represent the data. The shaded histogram is the background shape predicted by the Monte Carlo calculation. The solid line is the fit of the data to two Gaussian functions plus the background histogram.

predicted for the six decay paths shown in Figure 8, including background, for right and wrong  $K$ - $\ell$  sign combinations. A  $\chi^2$  function is formed with floating  $B^{**}$  fraction  $h^{**}$  and hadronization amplitudes. For luminosity  $110 \text{ pb}^{-1}$ , we find  $h^{**} = 0.28 \pm 0.06 \pm 0.03$ . Assuming calculated mass splittings and relative production rates for the four states determined by spin counting, we find the mass of the narrowest state to be  $m(B_1(J=1, j_q=3/2)) = (5.71 \pm 0.02) \text{ GeV}/c^2$ , consistent with predictions<sup>6</sup> and with observations at LEP.

## 2.6 Transverse Momentum and Total Cross Section of $e^+e^-$ Pairs with Invariant Mass in the $Z$ Region

Initial state radiation gives Drell-Yan pairs produced in hadronic collisions a  $p_T$  and companion jets. Predictions for the production properties of the pairs are finite and physical at all  $p_T$ . The phenomena at low  $p_T$  are non-perturbative and so must be measured. This analysis [7] requires the presence of two or more isolated, well-identified electrons of high transverse energy  $E_T$  (the precise value of the minimum allowed  $E_T$  depends upon the region of the detector in which the electron track is found) in the dataset of central electron triggers. Cuts that require the invariant mass of each electron pair to lie in the range  $66\text{--}116 \text{ GeV}/c^2$  ensure its consistency with the mass of the  $Z^0$ . After subtraction of the small background associated with  $e^+e^-$  pairs from  $W^+W^-$ ,  $\tau^+\tau^-$ , and heavy quark decays, the events are binned in  $p_T$  and the average value of the cross section measured for each bin is corrected to the value at bin center. Acceptance corrections are made with simulated data from the Monte Carlo generator PYTHIA, which generates the decay with leading-order production matrix elements and initial state radiation via parton shower algorithms. Higher order QCD corrections are approximated by weighting events with the factor

$$K(M^2) = 1 + \frac{4}{3}(1 + \frac{4}{3}\pi^2)\alpha_s(M^2)/2\pi.$$

The two-loop value of  $\alpha_s$  is used. For  $M > 50 \text{ GeV}/c^2$ ,  $1.25 < K < 1.36$ . Final state radiation is predicted with the Monte Carlo program PHOTOS, and CTEQ3L PDF's are used. Independent measurements are made for three classes of events: ones with two central electrons, ones with a central and a forward

<sup>6</sup>E. Eichten, C. Hill, and C. Quigg, Phys. Rev. Lett. **71**, 25 (1993).

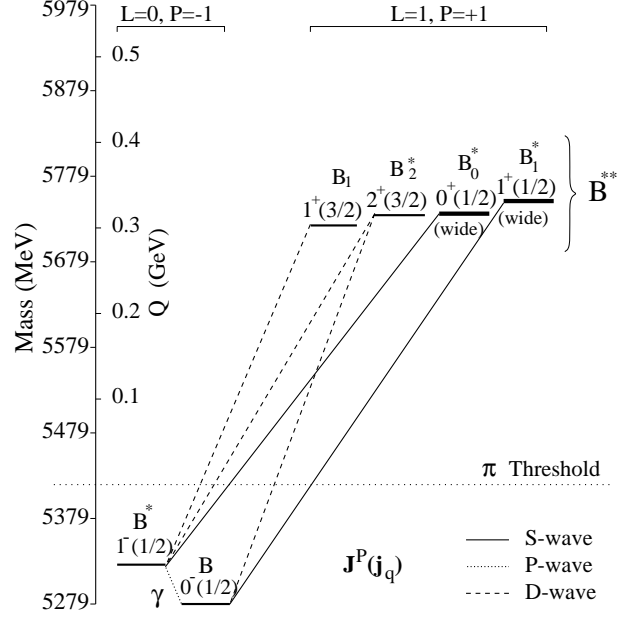


Figure 7: The predicted spectrum and dominant decays of the low-lying  $B$  meson states.

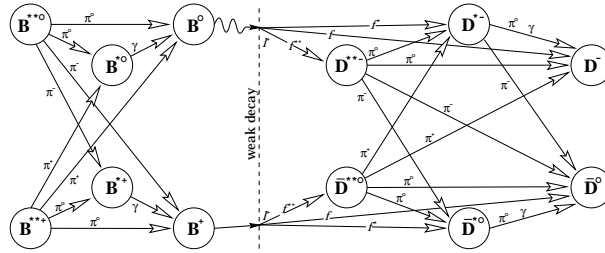


Figure 8: The transitions that contribute to the  $\ell^+ D^{(*)}$  samples. The left side portrays the strong decays of excited  $B$  mesons to the ground state; the weak semileptonic decays of the  $B^{0,+}$  are shown in the center; and the right side shows the decay paths of the charm mesons that result.

electron, and ones with a central and a plug electron. Background is estimated with  $e\mu$  pairs. The total cross section for these events is measured, for a luminosity of  $110 \text{ pb}^{-1}$ , to be  $248 \pm 4 \pm 3 \pm 10 \text{ pb}$ , where the first error concerns statistics and efficiency, the second concerns systematics associated with background subtraction and acceptance, and the third concerns the luminosity. This result is consistent with theoretical expectations obtained with EV, which predicts  $\sigma = 231 \text{ pb}$  with CTEQ4M and  $\sigma = 225 \text{ pb}$  with MRS-R2. A prediction of  $\sigma = 233 \text{ pb}$  made using RESBOS is also consistent. A related measurement of the differential cross section  $d\sigma/dp_T$  is also consistent with theoretical expectations and with previous measurements and provides improved precision over that of previous studies. Figure 9 shows this result.

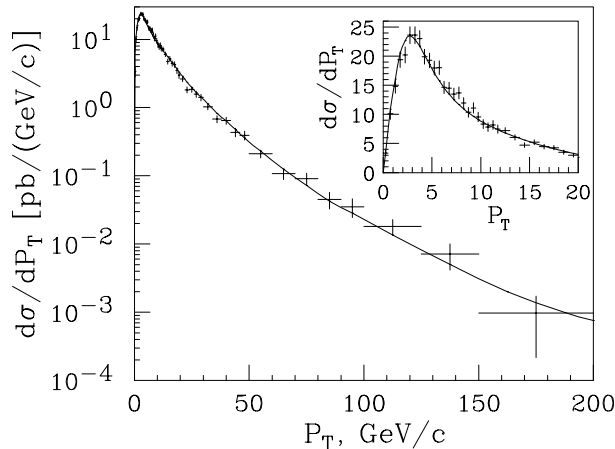


Figure 9: The differential cross section with respect to  $p_T$  of  $e^+e^-$  pairs in the mass range  $66\text{-}116 \text{ GeV}/c^2$ . The crosses are the data, and the curve is the RESBOS  $Z$ -only calculation normalized to the data. The insert shows the  $p_T < 20 \text{ GeV}/c$  region with a linear ordinate. The data errors do not include the 3.9% luminosity error.

## 2.7 $d\sigma/dy$ of $e^+e^-$ Pairs with Invariant Mass in the $Z$ Region

The momentum fractions  $x_1$  and  $x_2$  of a colliding quark and antiquark are related to the rapidity  $y$  of an intermediate  $\gamma^*$  or  $Z$  boson through

$$x_{1,2} = \left(\frac{M}{\sqrt{s}}\right)e^{\pm y},$$

where  $M$  is the mass of the  $e^+e^-$  pair produced by the boson decay. Consequently a large measured value of  $y$  indicates the presence of a system in which one parton has large  $x$ , the other, small. This measurement [8] of the differential cross section  $d\sigma/dy$  of the  $e^+e^-$  pairs tests the effect of missing next-to-next-to-leading order terms<sup>7</sup> and power correction terms<sup>8</sup> in the QCD calculation. The measurement proceeds in a manner similar to the one in the previous section, with the inclusion of two additional classes of events: those in which both electrons are observed in the plug, and those in which one is in the plug and one in the forward region. These additional classes permit measurements for  $Z$  bosons with  $|y|$  up to 2.8. The trigger requires one central or one plug electron. Examination of  $108 \text{ pb}^{-1}$  of data indicates good agreement with NLO QCD for both the MRST99 and CTEQ5M-1 PDF's. The differential cross sections in the  $Z$  mass range and above it are shown in Figures 10 and 11.

<sup>7</sup>R. Hamburg, W.L. van Neerven, and T. Matsuura, Nucl. Phys. B **359**, 343 (1991); W.L. van Neerven and E.B. Zijlstra, Nucl. Phys. B **382**, 11 (1992); U.K. Yang and A. Bodek, Euro. Phys. Jour. C **13**, 241 (2000); W.L. van Neerven and A. Vogt, Nucl. Phys. B **568**, 263 (2000).

<sup>8</sup>M. Dasgupta, J. High Energy Phys. 12 (1999) 008.



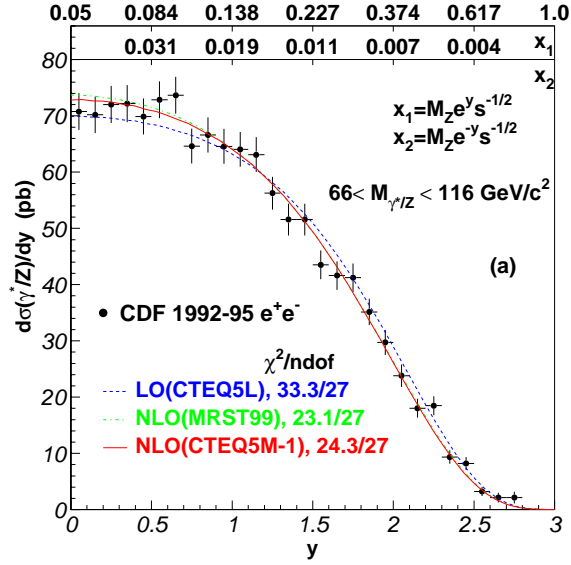


Figure 10: The differential cross section with respect to rapidity of  $e^+e^-$  pairs in the mass range 66-116  $\text{GeV}/c^2$ . The error bars include statistical errors only. The theoretical prediction has been normalized to the data in the  $Z$  boson mass region.

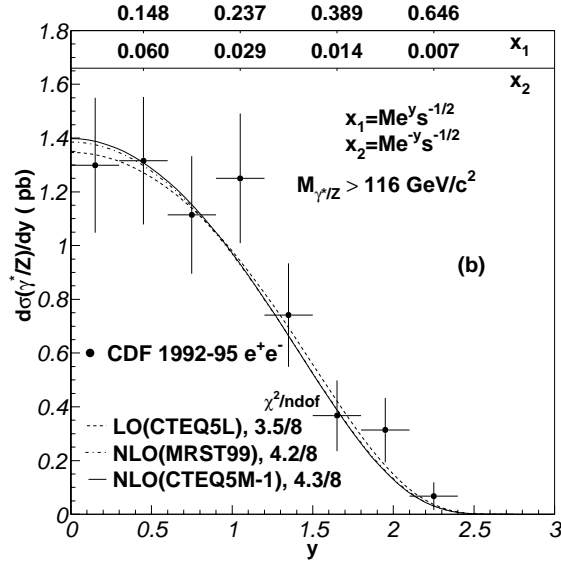


Figure 11: The differential cross section with respect to  $p_T$  of  $e^+e^-$  pairs in the mass range  $> 116 \text{ GeV}/c^2$ . The  $M$  used to obtain  $x_1$  and  $x_2$  is the mean mass over the bin. The error bars include statistical errors only. The theoretical prediction has been normalized to the data in the  $Z$  boson mass region.

### 3 Searches for New Particles

#### 3.1 Technicolor

##### 3.1.1 Technirho and Technipion

Technicolor associates electroweak symmetry breaking with the existence of states of two techniquarks (called the technipions,  $\pi_T$ ) bound by the technicolor force. In Walking Technicolor,<sup>9</sup> color singlet technirhos,  $\rho_T$ , can be produced in  $s$ -channel  $q\bar{q}$  annihilation. CDF has searched [9] for  $\pi_T$  and  $\rho_T$  in final states with four jets and in final states with a lepton, two jets, and missing  $E_T$ ,  $\cancel{E}_T$ . The channels examined are (1)  $\rho_T^{\pm,0} \rightarrow \pi_T^{\pm} \pi_T^{0,\mp}$ ;  $\pi_T^{\pm} \rightarrow \bar{b}c$ ;  $\pi_T^{0,\mp} \rightarrow b\bar{b}$  or  $\bar{b}c$  and (2)  $\rho_T^{\pm,0} \rightarrow W^{\pm} \pi_T^{0,\mp}$ ;  $W^{\pm} \rightarrow \ell^{\pm} \nu$  or  $q\bar{q}$ ;  $\pi_T^{0,\mp} \rightarrow b\bar{b}$  or  $\bar{b}c$ . In the lepton plus two jets mode, events which satisfy the trigger on an isolated central electron or muon with  $p_T > 20$  GeV are examined and required to have  $\cancel{E}_T > 20$  GeV and two jets, at least one of which has been tagged by its secondary vertex information as being produced by a  $b$  quark. Because the technicolor particle masses are expected to be related such that  $M(\pi_T) + M(W) \approx M(\rho_T)$ , the  $\pi_T$  should be produced almost at rest. The  $p_T$  of the two jets they produce during decay,  $p_T(jj)$ , should consequently be smaller than that of background jet pairs, and the jets should be almost back to back. Consequently cuts are placed on the included angle  $\Delta\phi(jj)$  and on  $p_T(jj)$ . The mass of the two-jet system,  $M(jj)$ , is reconstructed. Reconstructing the mass of the system of  $W$  and two jets,  $M(Wjj)$ , requires the longitudinal momentum of the neutrino,  $p_z(\nu)$ , which is obtained by constraining the lepton-neutrino system mass to the  $W$  mass. Cuts determined by Monte Carlo simulation are placed at three standard deviations above and below the reconstructed masses. A total of 47 combinations of  $\rho_T$  and  $\pi_T$  masses for which the cross section is expected to be greater than 5 pb are examined. The data are compared to theoretical predictions for  $N_{TC}$ (number of technicolors) = 4,  $Q_D$ (techniquark charge) = 1/3, and  $\sin\chi$ (the mixing angle) = 1/3. Events containing  $W\bar{b}b$ ,  $W\bar{c}c$ , and  $Wc$  are the principal background. The primary sources of systematic error are initial and final state radiation. No excess is observed above background for 109 pb<sup>-1</sup> of data. Figure 12 shows the excluded region of parameter space. A shape analysis of the four-jet events provides no additional constraints.

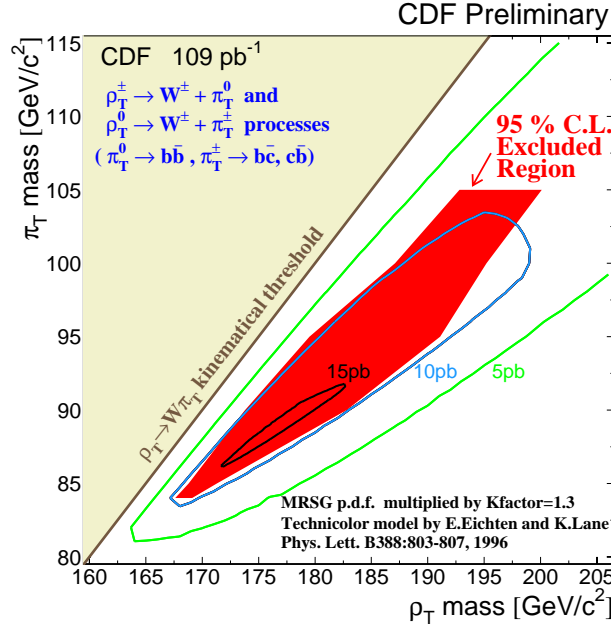


Figure 12: The shaded region shows the 95% C.L. excluded region in the  $m_{\pi_T} - m_{\rho_T}$  plane. Three contours of  $\sigma^{\text{theory}}$  are also shown. PYTHIA version 6.1 with PDF MRSG and K-factor 1.3 was used to calculate the cross section.

<sup>9</sup>E. Eichten and K. Lane, Phys. Lett. B **388**, 803 (1996), and references therein.

### 3.1.2 Leptophobic $Z'$

Topcolor-assisted technicolor (TAT)<sup>10</sup> accounts for the large mass of the top by proposing a residual global symmetry  $SU(3) \times U(1)$  below 1 TeV. The  $U(1)$  can produce a  $Z'$  which in one model<sup>11</sup> is “leptophobic”: it decays purely to quarks and produces the sequence  $Z' \rightarrow t\bar{t} \rightarrow WWbb$ ;  $W \rightarrow q\bar{q}$ ;  $W \rightarrow \ell\nu$ . The search [10] for this  $Z'$  examines events from the trigger on central, isolated, high- $E_T$  leptons, and begins by identifying those with four associated jets, at least one of which has been tagged as a  $b$ . These events have the “lepton + jets” signature, which is used in a variety of analysis involving the top. We require that  $\cancel{E}_T > 20$  GeV. Constraining the masses  $M(q\bar{q})$  and  $M(\ell\nu)$  to be equal to  $M(W)$  provides the longitudinal momentum of the neutrino.  $M(Wb)$  is constrained to the most recent measurement of the top mass, 175 GeV/ $c^2$ . A kinematic fit of the  $t\bar{t}$  pair is used to extract the  $t$  and  $\bar{t}$  momenta, which are used to compute the mass  $M(t\bar{t})$  shown in Figure 13.  $W$  + jets events are the principal background, and systematic uncertainties are principally due to the evaluation of the jet  $E_T$  scale, initial and final state gluon radiation, the measured mass of the top, the luminosity, and the choice of PDF. For 106 pb<sup>-1</sup> of data, no excess is observed above expectations for Standard Model top production. Figure 14 compares the associated 95% C.L. upper limits on  $\sigma \times BR(X \rightarrow t\bar{t})$  to theoretical predictions, as a function of mass of the  $Z'$ , for two assumed widths.

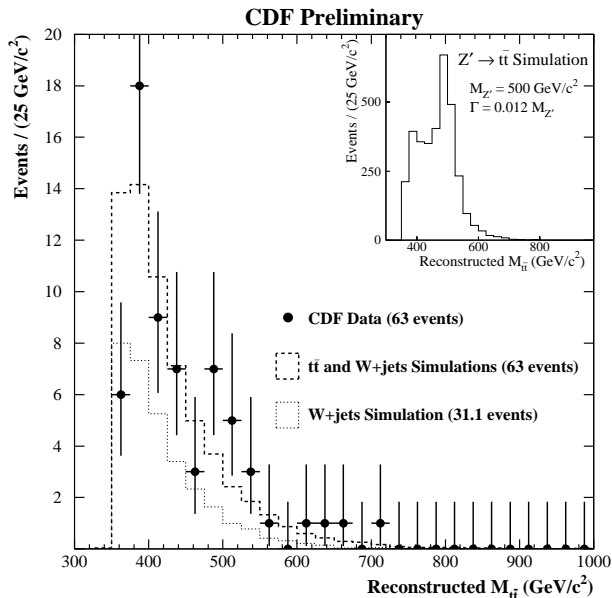


Figure 13: The observed  $M_{t\bar{t}}$  spectrum (points) compared to the QCD  $W$  + jets background (fine dashes) and the total Standard Model prediction including both QCD  $W$  + jets and  $t\bar{t}$  production (thick dashes). The  $t\bar{t}$  prediction has been normalized such that the number of events in the total Standard Model prediction is equal to the number of events in the data. The inset shows the expected  $M_{t\bar{t}}$  shape resulting from simulation of a narrow vector  $X \rightarrow t\bar{t}$  resonance with  $M_X = 500$  GeV/ $c^2$  and  $\Gamma = 0.012M_X$  in the CDF detector.

### 3.1.3 Second and Third Generation Leptoquarks

Leptoquarks are a natural element of many unification schemes. Technirhos,  $\rho_{T8}$ , couple to the gluon and so may be produced at the Tevatron. Technirhos may decay to pairs of color triplet technipions,  $\pi_{LQ}$ , which are scalar leptoquarks. CDF has searched [11] for the decays  $\pi_{LQ} \rightarrow c\bar{\nu}$  and  $\pi_{LQ} \rightarrow b\bar{\nu}$ , for which the  $\pi_{LQ}$  are treated as second and third generation objects, respectively. We examine events for which  $\cancel{E}_T > 35$  GeV, and select those with 2–3 jets of  $E_T \geq 15$  GeV and  $|\eta| \leq 2$ . These requirements

<sup>10</sup>C.T. Hill, Phys. Lett. B **345**, 483 (1995); C.T. Hill and S.J. Parke, Phys. Rev. D **49**, 4454 (1994).

<sup>11</sup>R.M. Harris, C.T. Hill, and S.J. Parke, FERMILAB-FN-687 (1999).

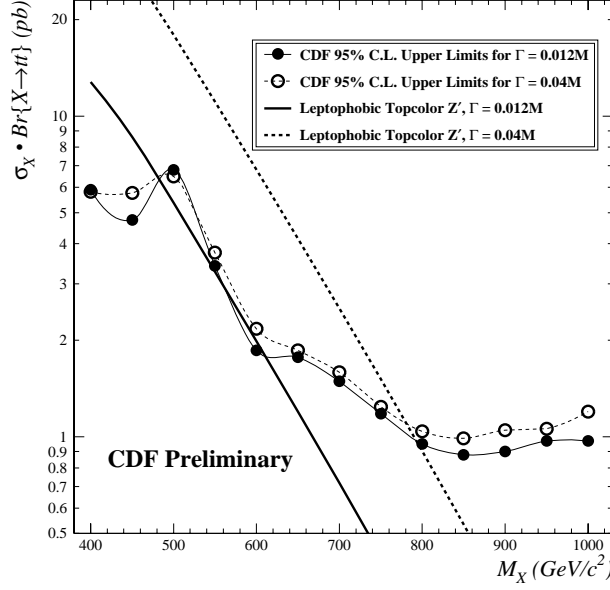


Figure 14: The 95% C.L. upper limits on  $\sigma_X \times BR(X \rightarrow t\bar{t})$  as a function of mass, compared to the cross section for a leptophobic topcolor  $Z'$  for two resonance widths.

reduce background from  $t\bar{t}$  decays, which typically produce four or more jets. We also require that no additional jets with  $E_T > 7$  GeV and  $|\eta| \leq 3.6$  be present, to suppress background from QCD gluon radiation.  $\cancel{E}_T$  is required to be greater than 40 GeV to reduce the systematic uncertainty associated with the energy threshold. To reduce the effect of energy mismeasurements (which produce  $\cancel{E}_T$  parallel or anti-parallel to jets), the angles  $\Delta\phi$  between  $\cancel{E}_T$  and jets are restricted such that  $\Delta\phi(\cancel{E}_T, \text{any jet}) > 45^\circ$  and  $\Delta\phi(\cancel{E}_T, \text{leading jet}) < 165^\circ$ . To suppress QCD background, the further requirement is made that  $45^\circ < \Delta\phi(\text{jet1}, \text{jet2}) < 165^\circ$ , where jets are enumerated in order of decreasing energy. The  $b$  and  $c$  jets are tagged with a variable known as jet probability, which is related to their impact parameters. Backgrounds from QCD processes and from  $W(\rightarrow \tau \rightarrow \text{hadrons}) + \text{jet}$  are predicted by simulation. The signal is simulated under the assumption that the leptoquarks have no coupling to charged leptons:  $\beta = 0$ . An examination of  $88 \text{ pb}^{-1}$  of data indicates no excess above background. Background-subtracted 95% C.L. limits on the masses  $M$  of continuum-produced leptoquarks are as follows: for second (third) generation scalar<sup>12</sup> leptoquarks,  $M > 123(148)$  GeV; for second (third) generation minimally coupled vector<sup>13</sup> leptoquarks,  $M > 171(199)$  GeV; for second (third) generation Yang-Mills vector<sup>12</sup> leptoquarks,  $M > 222(250)$  GeV. For technicolor-produced scalar leptoquarks, the production cross section depends on the mass of the  $\rho_{T8}$  and the mass difference  $\Delta M \equiv M(\pi_{T8}) - M(\pi_{LQ})$ . For second (third) generation technicolor-produced scalar leptoquarks,  $M(\rho_{T8}) > 510(600)$  GeV for  $\Delta M = 0$ . Figures 15 and 16 show the 95% C.L. limits on leptoquark production cross section as a function of leptoquark mass for second and third generations, respectively.

### 3.2 Search for a $W'$ Boson

In this direct search [12] for the propagator of a new force, we look for evidence of the process  $p\bar{p} \rightarrow W'X$ ;  $W' \rightarrow \mu\nu$  and assume that the channel  $W' \rightarrow WZ^0$  is suppressed.<sup>14</sup> The analysis considers events saved by the muon trigger, and requires that the  $p_T$  and  $\cancel{E}_T$  of the muon exceed 20 GeV/ $c$  and 20 GeV, respectively. The muon is required to be isolated (this rejects misidentified jets) and to have energy consistent with that of a minimum ionizing particle. Drell-Yan events are vetoed, and cosmic ray muons are rejected by timing. We define the azimuthal angle between the muon and the direction of the  $\cancel{E}_T$

<sup>12</sup>M. Krämer, T. Plehn, and P. Zerwas, Phys. Rev. Lett. **79**, 341 (1997).

<sup>13</sup>J. Blümlein, E. Boos, and A. Kryukov, Z. Phys. **C76**, 137 (1997).

<sup>14</sup>G. Altarelli *et al.*, Z. Phys. C **45**, 109 (1989).

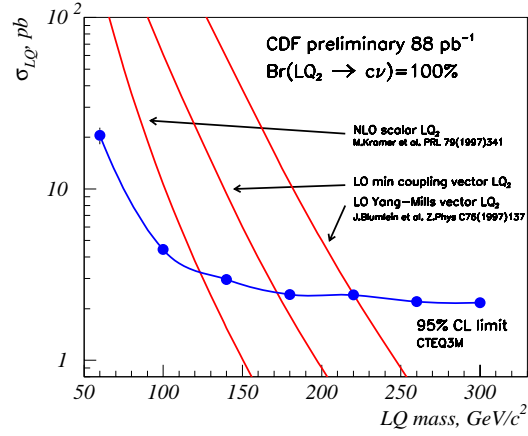


Figure 15: The 95% C.L. limit for scalar and vector second generation leptoquarks assuming  $\beta = 0$ , compared to theoretical calculations.

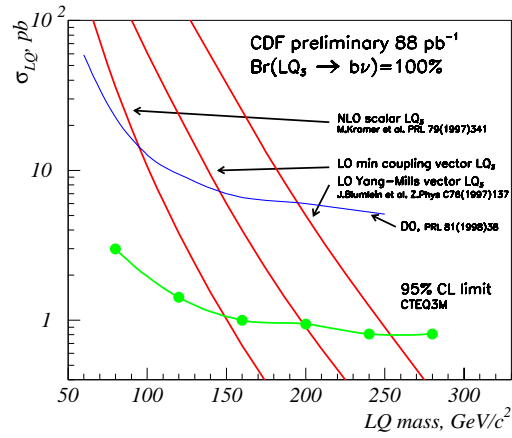


Figure 16: The 95% C.L. limit for scalar and vector third generation leptoquarks assuming  $\beta = 0$ , compared to theoretical calculations. The D0 Collaboration results are also shown.

to be  $\phi_{\mu\nu}$ , and we compute  $M_T \equiv \sqrt{2p_T^\mu \cancel{E}_T (1 - \cos\phi_{\mu\nu})}$ . Background is due to  $W$  and  $Z$  decays that produce muons (either directly or by cascade), muons from top decays, and fakes. A NLO theoretical calculation<sup>15</sup> is used to predict the  $p_T$  and  $\eta$  distributions of both the  $W'$  signal and the background with the CTEQ4A1 PDF and  $q^2 = M_{W'}^2$ , and PYTHIA is used to predict their  $M_T$  distributions. The measured  $M_T$  distribution is fitted with a likelihood function that includes the  $W'$ , background from  $W$ , and other backgrounds. Systematic uncertainties are associated with choice of PDF, acceptance, and track  $p_T$  resolution. No excess is observed at the large  $M_T$  values where a  $W'$  signal would be expected. A small excess around  $M_T = 200$  GeV (see Figure 17) is not statistically significant. The width of the expected signal distribution is dominated by detector resolution for  $W'$  masses above 300 GeV/c<sup>2</sup>. Upper limits on the  $W'$  cross section as a function of  $W'$  mass are shown in Figure 18; these exclude  $W'$  masses less than 660 GeV/c<sup>2</sup> at 95% C.L.

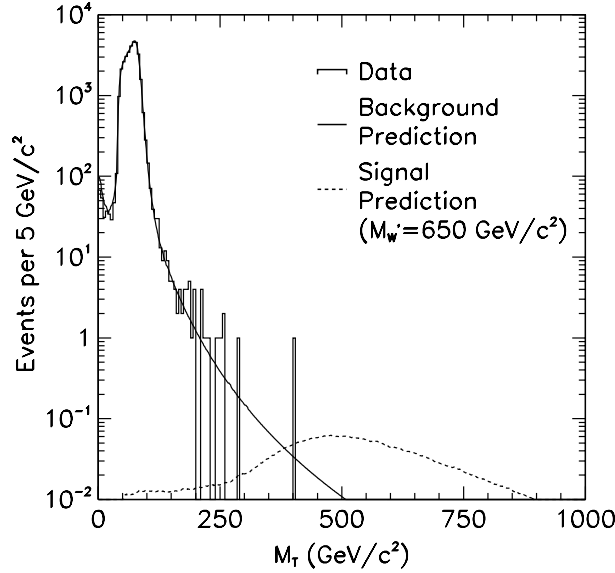


Figure 17: The transverse mass spectrum of the  $\mu\nu_\mu$  candidate events. The distribution expected from the production of a  $W'$  boson with a mass of 650 GeV/c<sup>2</sup> is illustrated by the dashed distribution.

### 3.3 Search for a Fourth Generation Quark, $b'$

This search [13] for pair-produced fourth generation quarks considers the decay sequence  $b'\bar{b}' \rightarrow Z^0 Z^0 b\bar{b}$ ;  $Z^0 \rightarrow \text{jets}$ ;  $Z^0 \rightarrow \ell\ell\nu\nu$ . This decay mode is favored<sup>16</sup> if the mass relations  $m(b') < m(t)$  and  $m(b') < m(t')$  hold (so  $b' \rightarrow tW^-$  and  $b' \rightarrow t'W^-$  are forbidden, respectively) and if the decay  $b' \rightarrow bH$  is suppressed. In this case  $b' \rightarrow cW^-$  is doubly Cabibbo suppressed, so if the CKM matrix element ratio  $V_{cb'}/V_{tb'} < 10^{-2}$ ,  $b' \rightarrow bZ^0$  dominates up to  $m_{b'} \simeq 230$  GeV/c<sup>2</sup>. This is a loop-induced flavor-changing neutral current. The high- $p_T$  central lepton trigger is used. We identify two leptons ( $\ell\ell$ ) in an event and reconstruct the mass  $M(\ell\ell)$ . The event is saved if  $M(\ell\ell)$  is within 15 GeV/c<sup>2</sup> of the  $Z^0$  mass. The event is required to have at least three jets, one of which has been tagged as a  $b$ . A set of masses  $m_{b'}$  is considered such that, for jets with  $E_T > 15$  GeV and  $|\eta| < 2$ ,

$$\sum_{\text{jets}} E_T > (m_{b'} c^2 - 60 \text{ GeV}).$$

The only non-negligible background to this analysis is  $Z^0$  events with associated QCD hadronic jets. This is estimated with the Monte Carlo programs VECBOS (for leading-order matrix elements for  $Z^0 + 3$  parton

<sup>15</sup>P.B. Arnold and R.P. Kauffman, Nucl. Phys. B **349**, 381 (1991); G.A. Ladinsky and C.-P. Yuan, Phys. Rev. D **50**, 4239 (1994).

<sup>16</sup>W.S. Hou and R.G. Stuart, Nucl. Phys. B **320**, 277 (1989); W.S. Hou and R.G. Stuart, Phys. Rev. Lett. **62**, 617 (1989).

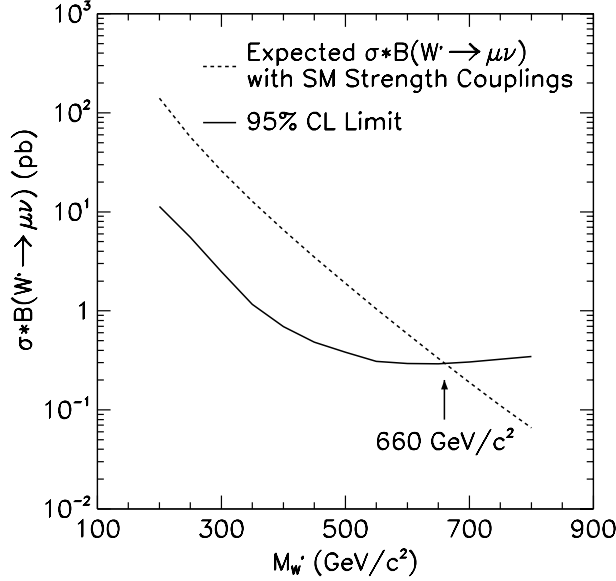


Figure 18: The upper limits on the  $W'$  boson production cross section as a function of the  $W'$  boson mass.

events and HERWIG (for gluon radiation and hadronic fragmentation). The MRSD0' PDF is used. The principal systematics are associated with jet energy scale and gluon radiation. As Figure 19 shows, no signal is evident in  $88 \text{ pb}^{-1}$  luminosity of collisions; one  $\mu\mu$  pair is observed while two background events are expected. With no background subtraction, and using a particular NLO calculation<sup>17</sup> and the assumption that the branching ratio for  $b' \rightarrow bZ^0$  equals 1, CDF extracts a 95% C.L. limit on  $\sigma_{p\bar{p} \rightarrow b'\bar{b}'} \times [BR(b' \rightarrow bZ^0)]^2$  as a function of  $m_{b'}$ , and excludes (see Figure 20)  $b'$  masses from 100 to 199  $\text{GeV}/c^2$ .

### 3.4 Supersymmetry

#### 3.4.1 Gravitino Production and Other Processes with Large Missing Transverse Energy

A search [14] was conducted for the spin-3/2 supersymmetric (SUSY) partner of the graviton.<sup>18</sup> The following channels were examined:

$$\begin{aligned}
 q\bar{q} &\rightarrow \tilde{G}\tilde{G}g \\
 qg &\rightarrow \tilde{G}\tilde{G}q \\
 \bar{q}g &\rightarrow \tilde{G}\tilde{G}\bar{q} \\
 gg &\rightarrow \tilde{G}\tilde{G}g \\
 q\bar{q} &\rightarrow \tilde{G}\tilde{G}\gamma.
 \end{aligned} \tag{2}$$

If the mass  $m(\tilde{G}) \ll 10^{-4} \text{ eV}/c^2$  (the gravitino  $\tilde{G}$  is then the LSP), these channels may be observed at the Tevatron through  $\cancel{E}_T$ . The trigger for this study requires that  $\cancel{E}_T > 35 \text{ GeV}$ , where the transverse energy is summed over all calorimeter cells with  $|\eta| < 3.6$ . We require that an event have  $\cancel{E}_T > 50 \text{ GeV}$  and one central jet with  $E_T > 10 \text{ GeV}$ . The most energetic jet (at any  $\eta$ ) must have at least 80  $\text{GeV}$ . Events with high  $p_T$  leptons are rejected. The angle between the  $\cancel{E}_T$  vector and the nearest jet is required to be  $\geq 90^\circ$  to remove most instrumental effects; additional instrumental effects are removed by requiring that the tracks have energy ratio  $E_{\text{EM}}/E_{\text{total}} < 0.95$  and by rejecting isolated tracks with  $p_T > 30 \text{ GeV}/c$ . Backgrounds to this search include  $W/Z + \text{jet}$  events (whose rate is estimated with PYTHIA from CDF cross sections),  $t\bar{t} + WW$ ,  $WZ$ , or  $ZZ$  events (whose rate is estimated from theoretical models), and

<sup>17</sup>E. Laenen *et al.*, Phys. Lett. B **321**, 254 (1994).

<sup>18</sup>S. Dimopoulos, S. Thomas, and J.D. Wells, Nucl. Phys. B **488**, 39 (1997); G.F. Giudice and R. Rattazzi, hep-ph/9801271 and references therein.

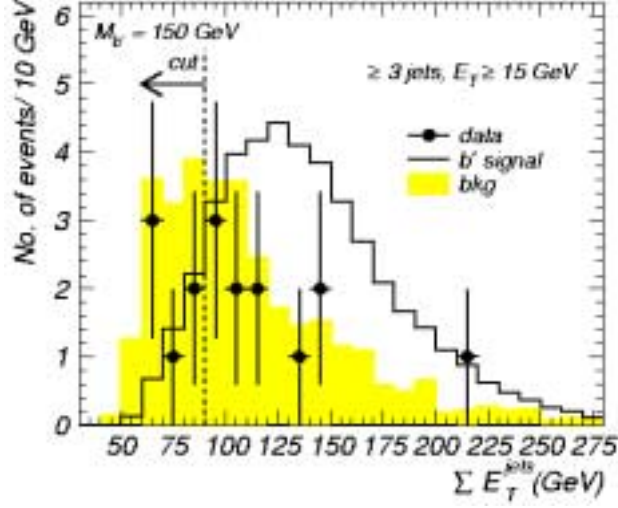


Figure 19: The  $\Sigma E_T^{\text{jets}}$  distribution for events with at least three jets with  $E_T > 15$  GeV and  $|\eta| < 2$ , before the  $b$ -tagging requirement. The expected Standard Model background is shown shaded. The expected signal distribution for a  $b'$  quark mass of 150 GeV/ $c^2$  is shown as a solid line. The vertical dashed line represents the  $\Sigma E_T^{\text{jets}}$  cut for this specific  $b'$  mass. Events to the right of this line are accepted.

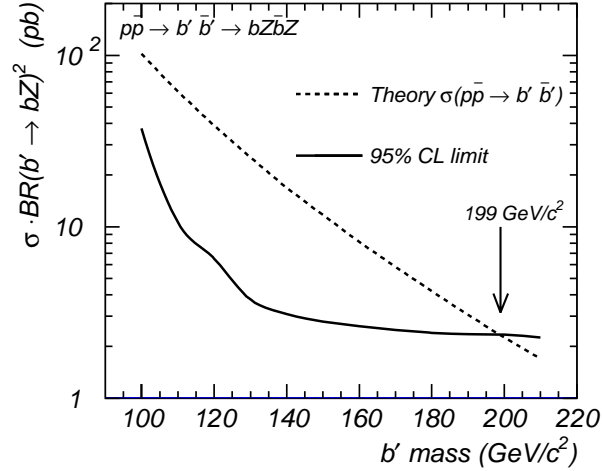


Figure 20: The 95% C.L. upper limit on the product of the  $p\bar{p} \rightarrow b'\bar{b'} X$  production cross section and the square of the branching ratio for the decay  $b' \rightarrow bZ^0$ . The dashed curve shows the predicted value for this product with the branching ratio set equal to 1 and the NLO production cross section mentioned in the main text.



mismeasured balanced QCD multijet events. The dominant systematic uncertainties are associated with knowledge of the production cross sections for backgrounds, the jet  $E_T$  scale, the collision luminosity, choice of renormalization and factorization scales  $\mu$  and PDF, and gluon radiation. As Figure 21 shows, no signal is observed. HERWIG is used to simulate gravitino production for the MRSD' PDF,  $\mu = E_T$ , and  $\sqrt{s} = 200$  GeV. The uncertainties on acceptance are convoluted with background estimates to derive upper limits on the cross section for the process  $p\bar{p} \rightarrow \tilde{G}\tilde{G} + \text{jet}$  ( $p_T^{\tilde{G}\tilde{G}} \geq 100$  GeV/c); these are shown in Figure 22. The most sensitive limit, at  $\cancel{E}_T \geq 175$  GeV, gives cross section  $\sigma \leq 3.1$  pb and mass  $m(\tilde{G}) \geq 1.1 \times 10^{-5}$  eV/c<sup>2</sup>.

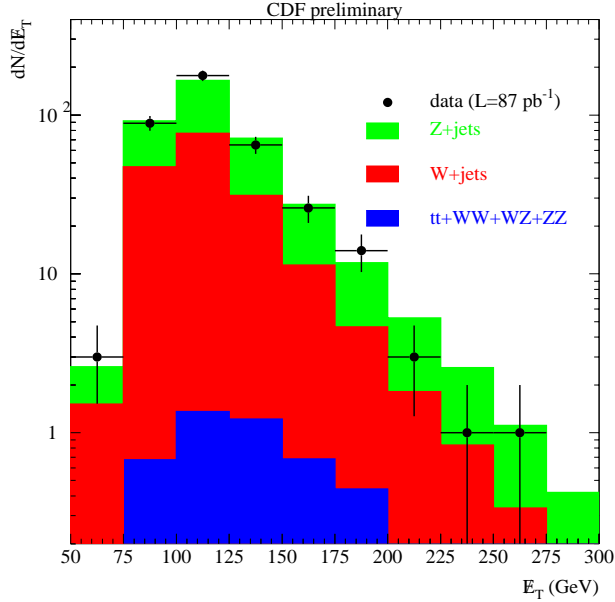


Figure 21: The distribution of  $\cancel{E}_T$  for data (points) compared to the central value expectations for  $Z + \text{jets}$ ,  $W + \text{jets}$ , and  $t\bar{t} + WW + WZ + ZZ$  events.

### 3.4.2 Search for Scalar Top and Scalar Bottom Quarks

A search [15] for the SUSY partners of  $t$  and  $b$ , respectively  $\tilde{t}$  and  $\tilde{b}$ , has been made. The  $\tilde{t}$  mass may be lower<sup>19</sup> than that of the  $t$  due to the strong Yukawa coupling associated with the large  $t$  mass. In some regions of SUSY parameter space, the mixing between  $\tilde{b}_L$  and  $\tilde{b}_R$  may be large, leading to large splitting between mass eigenstates and a consequently low value<sup>20</sup> for the mass of the  $\tilde{b}_1$ . We consider the channels  $p\bar{p} \rightarrow \tilde{t}_1\tilde{t}_1^* \rightarrow (c\tilde{\chi}_1^0)(\bar{c}\tilde{\chi}_1^0)$  and  $p\bar{p} \rightarrow \tilde{b}_1\tilde{b}_1^* \rightarrow (b\tilde{\chi}_1^0)(\bar{b}\tilde{\chi}_1^0)$ . The  $\tilde{\chi}_1^0$  is assumed to be the lightest neutralino and to be stable. This analysis uses events saved by the trigger on  $\cancel{E}_T > 35$  GeV. We select events with 2–3 hard ( $E_T \geq 15$  GeV,  $|\eta| < 2$ ) jets and no soft ( $7 \leq E_T \leq 15$  GeV,  $|\eta| \leq 3.6$ ) jets and require that  $\cancel{E}_T > 40$  GeV. The angle between any jet and the  $\cancel{E}_T$  vector must be  $> 45^\circ$ , and (for the most energetic jet)  $< 165^\circ$  to suppress events with energy mismeasurements. To suppress QCD background we require that the angle between the first and second leading jet lie in the range  $45^\circ$  to  $165^\circ$ . Events with high  $p_T$  leptons are vetoed. Heavy quark jets are tagged by their impact parameter with the jet probability parameter  $P_{\text{jet}}$ . A low value of  $P_{\text{jet}}$  implies a high probability that a jet is due to a heavy quark. For the  $\tilde{t}$  and  $\tilde{b}$  analyses, we require  $P_{\text{jet}} \leq 0.05$  and  $P_{\text{jet}} \leq 0.01$ , respectively. The principal backgrounds are due to QCD multijet events with mismeasured energy and  $W + \text{jet}$  events in which the  $W$  decays to an unidentified lepton or to a  $\tau$  that decays hadronically. These are estimated using data and Monte Carlo. The principal systematics are associated with gluon radiation, uncertainty on the jet energy scale and trigger efficiencies, the choice of factorization and renormalization scales and PDF, multiple interactions,

<sup>19</sup>K. Hikasa and M. Kobayashi, Phys. Rev. D **36**, 724 (1987); H. Baer *et al.*, Phys. Rev. D **44**, 725 (1991); H. Baer, J. Sender, and X. Tata, Phys. Rev. D **50**, 4517 (1994).

<sup>20</sup>A. Bartl, W. Majerotto, and W. Porod, Z. Phys. C **64**, 499 (1994).

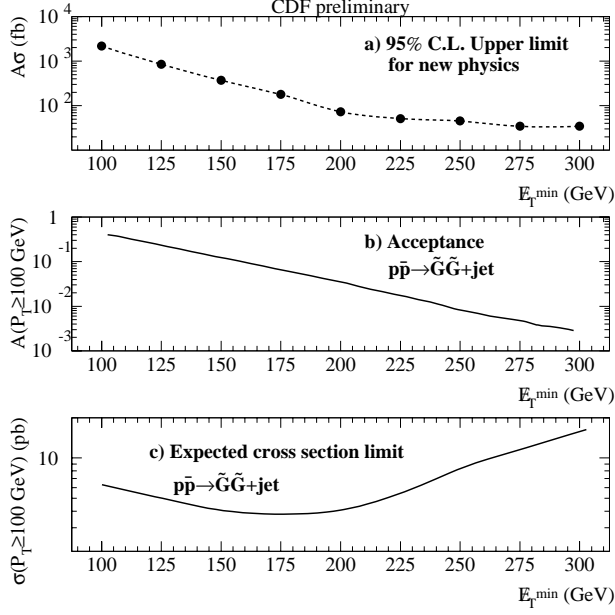


Figure 22: The 95% C.L. upper limit on the product of acceptance  $A$  and cross section  $\sigma$  for the production of new processes; the acceptance as a function of  $\cancel{E}_T$  for  $p\bar{p} \rightarrow \tilde{G}\tilde{G} + \text{jet}$  events produced with  $p_T(\tilde{G}\tilde{G}) > 100$  GeV/c; the 95% C.L. upper limit on the cross section for  $p\bar{p} \rightarrow \tilde{G}\tilde{G} + \text{jet}$  events produced with  $p_T(\tilde{G}\tilde{G}) > 100$  GeV/c expected for no signal.

the dependence of the cross sections upon the squark mass, luminosity, and Monte Carlo statistics. No excess of events was observed in either decay channel. Figure 23 shows the 95% C.L. exclusion region in  $m_{\tilde{\chi}_1^0} - m_{\tilde{t}_1}$  space, and Figure 24 shows the exclusion region for sbottom.

### 3.5 Search for the Charged Higgs Boson

The charged Higgs particle,  $H^\pm$ , may be observed through the decays  $t \rightarrow H^\pm b \rightarrow \tau^\pm \nu b$ , a channel favored<sup>21</sup> over  $t \rightarrow W^\pm b$  if  $m_{H^\pm} < (m_t - m_b)$  and  $\tan\beta$ , the ratio of the vacuum expectation values of the two Higgs doublets, is less than 1 or greater than 70 (see Figure 25). A study [16] was conducted for the cases  $m_{H^\pm} = 60, 100$ , and  $140$  GeV/c<sup>2</sup>. It assumes that  $t \rightarrow Hb$  and  $t \rightarrow Wb$  saturate the top branching ratios. The analysis begins with the selection of events with a lepton ( $e$  with  $E_T > 20$  GeV or  $\mu$  with  $p_T > 20$  GeV/c) in the central region of the detector as well as a central  $\tau$  with  $p_T > 15$  GeV/c, 2 jets, and a  $\cancel{E}_T$  significance,

$$S_{\cancel{E}_T} \equiv \frac{\cancel{E}_T}{\sqrt{\sum E_T (+p_T^\mu)}} > 3 \text{ for } e(\mu).$$

The cross section,  $\sigma(p\bar{p} \rightarrow t\bar{t})$ , is taken from the CDF measurements of top in the lepton + jets decay mode. The acceptance,  $A$ , is predicted with PYTHIA and TAUOLA for several branching ratios for  $t \rightarrow Hb$ . The expected number of events, computed as  $N = \sigma LA$  for collision luminosity  $L$ , is compared with data. Systematics on the measurement include uncertainty on the number of lepton + jet events, on the  $b$  tagging efficiency, and on  $\tau$  identification, as well as those arising from Monte Carlo statistics. The principal backgrounds are  $Z/\gamma \rightarrow \tau^+\tau^- + \text{jets}$  and  $Z/\gamma \rightarrow W + \text{three or more jets}$ , when the  $W$  is misidentified as a  $\tau$ . In a dataset of  $106 \text{ pb}^{-1}$ , four events are observed,  $3.1 \pm 0.5$  background events expected. We calculate an upper limit on the number of  $H^\pm$  events to be, at 95% C.L., 8.1 events. Figures 26 and 27 show the range of excluded mass as a function of branching ratio,  $BR(t \rightarrow Hb)$ , and  $\tan\beta$ , respectively.

<sup>21</sup>M. Drees and D.P. Roy, Phys. Lett. B **269**, 155 (1991); D.P. Roy, Phys. Lett. B **283**, 403 (1992).

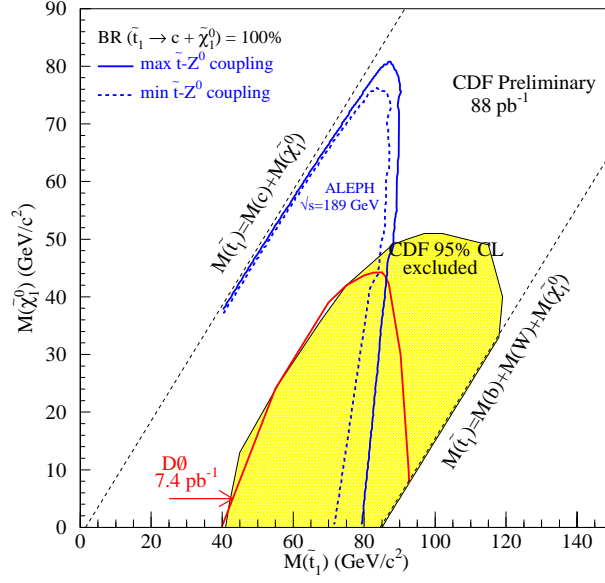


Figure 23: 95% C.L. exclusion region in the  $m_{\tilde{\chi}_1^0}$ - $m_{\tilde{t}_1}$  plane for the decay  $\tilde{t}_1 \rightarrow c \tilde{\chi}_1^0$ . Results by D0 and ALEPH are also shown.

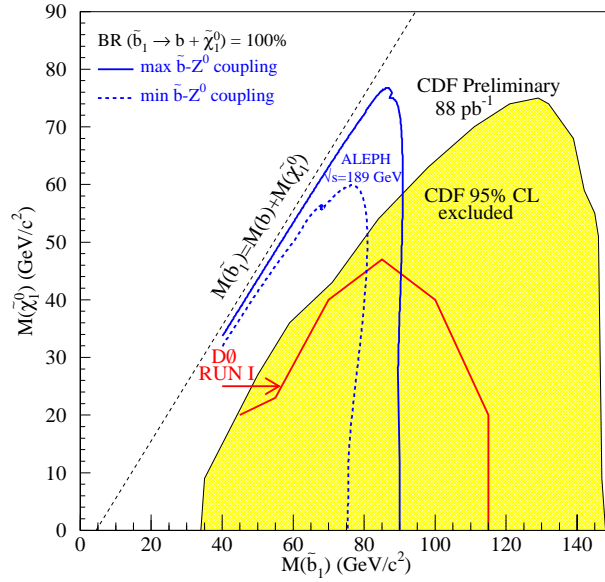


Figure 24: 95% C.L. exclusion region in the  $m_{\tilde{\chi}_1^0}$ - $m_{\tilde{b}_1}$  plane for the decay  $\tilde{b}_1 \rightarrow b \tilde{\chi}_1^0$ . Results by D0 and ALEPH are also shown.

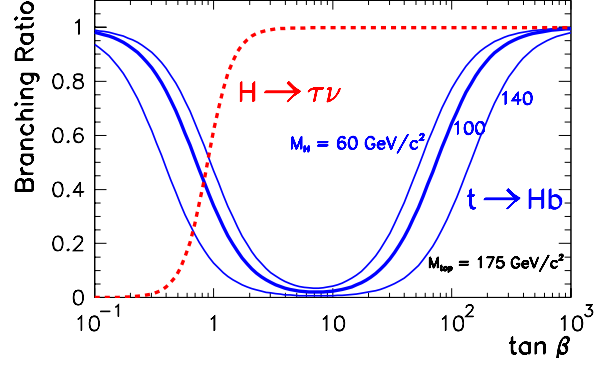


Figure 25: Branching fraction of  $H \rightarrow \tau\nu$  and  $t \rightarrow Hb$  as a function of  $\tan\beta$  at lowest order in the Minimal Supersymmetric Standard Model. The top quark mass is assumed to be  $175 \text{ GeV}/c^2$ .

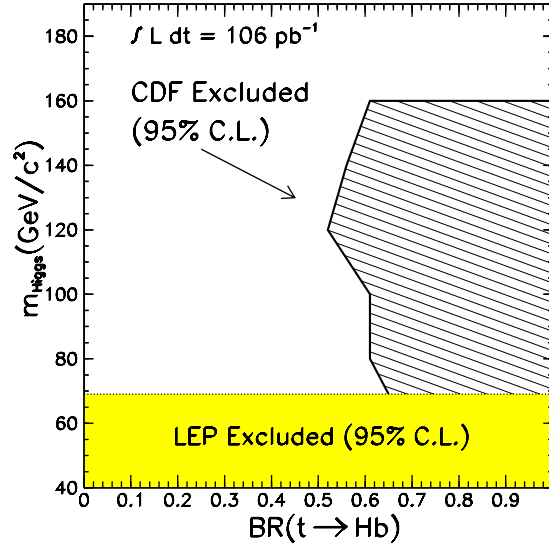


Figure 26: The region excluded at 95% C.L. for charged Higgs production versus the branching ratio for  $t \rightarrow H^+b$ .

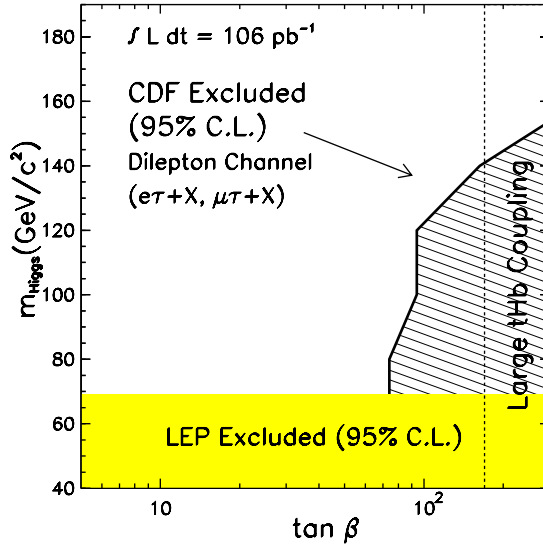


Figure 27: 95% C.L. excluded regions at different values of  $\tan\beta$  for charged Higgs production at lowest order in the Minimal Supersymmetric Standard Model. The coupling  $t\bar{b}H^+$  may become non-perturbative in the region at large values of  $\tan\beta$ , in which case the limit does not apply there.

## 4 Top Quark Studies

### 4.1 Helicity of $W$ Bosons as Measured with Top Quark Decays

A measurement [17] of the helicity of  $W$  bosons produced in decays  $t \rightarrow bW$ ;  $W \rightarrow \ell\nu$  tests whether the top decays are described by the universal  $V - A$  charged current interactions of the Standard Model. Because the amplitude for positive helicity  $W^+$  bosons is suppressed by chiral factors of order  $m_b^2/M_W^2$  (where  $m_b$  and  $M_W$  are the masses of the  $b$  and  $W$ , respectively), the  $W$  helicity is predominantly a superposition of zero and negative helicity states. The fraction of longitudinal (zero helicity)  $W$ 's in the top frame is predicted<sup>22</sup> to be

$$F_0 = \frac{m_t^2/2M_W^2}{1 + m_t^2/2M_W^2} = (70.1 \pm 1.6)\%$$

due to the large Yukawa coupling to the longitudinal mode of the  $W$ . The  $V - A$  coupling of the  $W$ -lepton vertex correlates the  $W$  helicity with the lepton momentum: as can be seen in Figure 28 (generated with a custom version of HERWIG), charged leptons from negative helicity  $W$ 's are expected to be softer than those from longitudinal  $W$ 's. This analysis considers two final states of the process  $t\bar{t} \rightarrow WWbb$ ; (1) that in which one  $W$  decays to  $q\bar{q}$ , the other to  $\ell\nu$ , and (2) that in which both  $W$ 's decay to  $\ell\nu$ . The first of these is saved by the lepton + jets trigger. The trigger for the second is two high- $p_T$  central leptons of different flavor and opposite charge, at least one of them isolated, as well as  $\cancel{E}_T > 35$  GeV and two jets.  $Z$  decays are vetoed. The principal backgrounds to the first channel are events in which  $W$  bosons are produced with associated jets and events with a fake lepton and jets. The principal backgrounds to the second channel are  $Z \rightarrow \tau\tau$ ,  $WW$ ,  $WZ$ , and  $ZZ$ . These are estimated with PYTHIA, ISAJET, and VECBOS. The analysis proceeds by simulating two samples of  $t \rightarrow Wb$  decays, those with longitudinal and those with negative helicity. Their lepton  $p_T$  distributions are parameterized. We weight the distributions by  $F_0$  and  $1 - F_0$  and sum them, then fit the result plus background to the data with a likelihood function. Systematic uncertainties include knowledge of the top mass (as this affects lepton  $p_T$ ), the shape and

<sup>22</sup>R. Peccei and X. Zhang, Nucl. Phys. B **337**, 269 (1990); G. Kane, C.-P. Yuan, and D. Ladinsky, Phys. Rev. D **45**, 124 (1992); R.H. Dalitz and G.R. Goldstein, Phys. Rev. D **45**, 1531 (1992); M. Jezabek and J.H. Kuhn, Phys. Lett. B **329**, 317 (1994); C.A. Nelson, B.T. Kress, M. Lopes, and T. McCauley, Phys. Rev. D **56**, 5928 (1997).

normalization of the background,  $b$ -tagging efficiency, Monte Carlo statistics, effects of gluon radiation, and choice of PDF. We find, for  $106 \text{ pb}^{-1}$  collision luminosity,  $F_0 = 0.91 \pm 0.37 \pm 0.13$ , consistent with the Standard Model prediction of 0.70. Figure 29 shows the fitted fraction  $F_0$  versus lepton  $p_T$  in each channel.

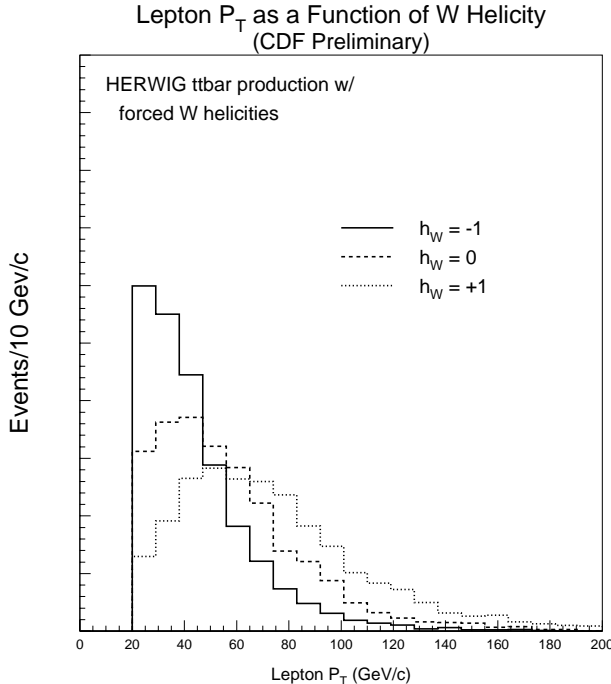


Figure 28: The lepton  $p_T$  distributions for the three  $W$  helicities. All three distributions are normalized to the same area.

## 4.2 Top $p_T$ Distribution

The Standard Model predicts that  $t\bar{t}$  is the dominant mechanism for top production. The existence of other<sup>23</sup> mechanisms could alter the top  $p_T$  spectrum, especially above 200 GeV/c, motivating this measurement. We consider events [18]  $t\bar{t} \rightarrow WWbb$  in which one  $W$  decays to  $q\bar{q}$ , the other to  $\ell\nu$ . These events are saved by the lepton + jets trigger. We require that all four jets be observed and that at least one jet be tagged as a  $b$  or that the jet with lowest  $E_T$  have  $E_T > 15 \text{ GeV}$  and  $|\eta| < 2$ . The top mass is constrained to  $175 \text{ GeV}/c^2$ , and the event is reconstructed. The  $p_T$  spectrum of the hadronic  $t$  (but not  $\bar{t}$ ) decays is measured. We correct for (“unsmeared”) effects of resolution and wrong track combinations. Backgrounds from  $W$  events associated with jets and from QCD multijet events in which one jet is misidentified as a lepton are estimated with VECBOS. An unbinned fit to the likelihood function  $L$  is performed, for  $L$  defined by

$$\ln L = \sum_{i=1}^{n_{data}} \left[ \ln \left( \sum_{j=1}^{n_{bin}} ((1-B)R_j T_j(p_T^i)) + BV(p_T^i) \right) \right] - \frac{(B - \mu_b)^2}{2\sigma^2(\mu_b)}.$$

Here  $B$  is the fitted background fraction,  $R_j$  is the fitted fraction of top quarks in true bin  $j$ ,  $T_j$  is the detector response function,  $V$  is the background template function, and  $\mu \pm \sigma$  is the estimated background fraction used to propagate the background uncertainties into the statistical uncertainty on  $R_j$ . We extract values of  $R_j$  for 4  $p_T$  bins and correct these for the fact that acceptance of top depends upon  $p_T$ . The Kolmogorov-Smirnov test is used to compare the result to a Standard Model calculation using

<sup>23</sup>C.T. Hill and S.J. Parke, Phys. Rev. D **49**, 4454 (1994); K. Lane, Phys. Rev. D **52**, 1546 (1995); T.G. Rizzo, hep-ph/9902273; E. Simmons, hep-ph/9908511.

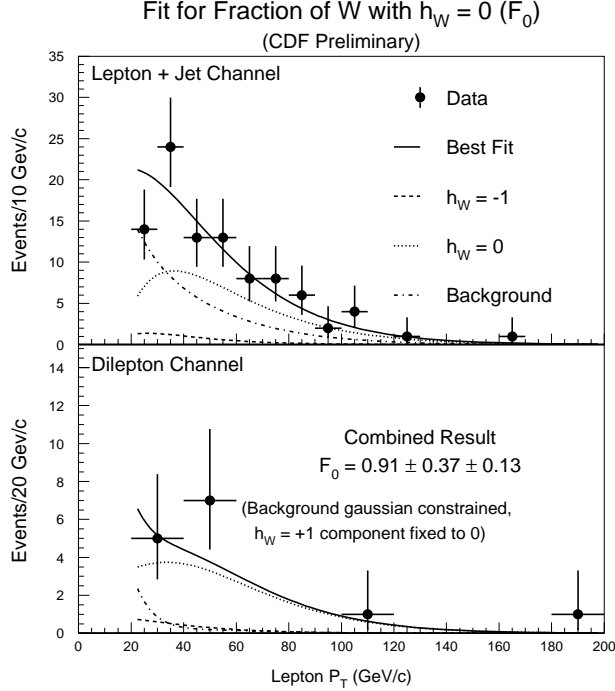


Figure 29: Lepton  $p_T$  distributions for the lepton + jet and dilepton subsamples. The data (points) are compared to the result of the combined fit (solid line) and to the background component of the fit (dashed line).

HERWIG and the MRSD0' PDF. Systematic uncertainties are associated with unsmeared parameters, gluon radiation, knowledge of the top mass, and acceptance. Figure 30 shows the result of this measurement, for  $106 \text{ pb}^{-1}$  luminosity of collisions. The probability to observe a difference as large as is shown is 5%; this probability varies from 1.0% to 9.4% for one standard deviation changes in the systematic errors. At 95% C.L., the fraction of top quarks with  $p_T$  in the range 225–425 GeV/c is  $< 0.16$ .

## 5 Direct Measurement of the $W$ Boson Width

The Breit-Wigner spectrum for lowest order diagrams of  $W$  production depends upon the width  $\Gamma_W$  of the  $W$  according to

$$\sigma(\hat{s}) \sim \frac{\hat{s}}{(\hat{s} - M_W^2)^2 + \hat{s}^2 \Gamma_W^2 / M_W^2},$$

where  $\sqrt{\hat{s}}$  is the  $\ell\nu$  mass in  $W \rightarrow \ell\nu$ . The Standard Model predicts

$$\begin{aligned} \Gamma_W &= \frac{\Gamma(W \rightarrow \ell\nu)}{BR(W \rightarrow \ell\nu)} \\ &= \frac{G_F M_W^3 / 6\sqrt{2}(1 + \delta_{SM})}{1/(3 + 6(1 + \alpha_s(M_W)/\pi) + O(\alpha_s^2))} \\ &= 2.093 \pm 0.002 \text{ GeV}. \end{aligned} \tag{3}$$

The radiative correction to the Born term,  $\delta_{SM}$ , has magnitude  $< 0.5\%$ . This analysis [19] considers the decay  $W \rightarrow (e \text{ or } \mu) + \nu$ . The triggers are (1) a central isolated well-identified  $e$  with  $E_T > 25 \text{ GeV}$  and  $p_T > 15 \text{ GeV/c}$  and (2) a central well-identified  $\mu$  with  $p_T > 25 \text{ GeV/c}$ .  $\cancel{E}_T$  must be  $> 25 \text{ GeV}$ . We define the recoil transverse energy vector,  $\vec{u} \equiv \sum_i E_i \sin\theta_i$ , where the sum is taken over calorimeter towers not traversed by the lepton, to  $|\eta| < 3.6$ . The vector  $-\vec{u}$ , which includes effects of initial state radiation, underlying event, and multiple interactions, estimates the  $p_T$  of the  $W$ . We require that  $|\vec{u}| < 20$

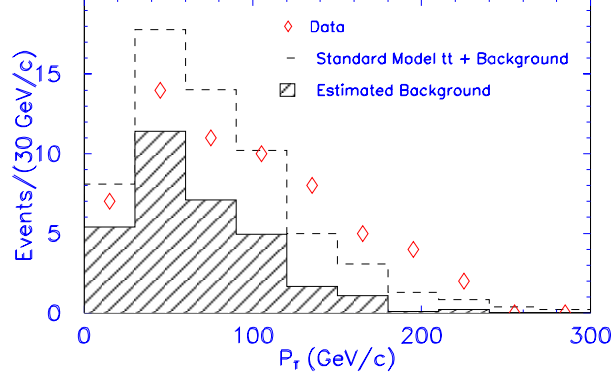


Figure 30: The measured  $p_T$  distribution for the hadronically decaying top quarks in the 61 event sample. The hatched distribution is the estimated background distribution, normalized to the estimated number of background events. The dashed distribution is the Standard Model prediction, normalized to the observed number of candidate events.

GeV. Leptons must be emitted at the primary vertex and must traverse the entire tracking chamber, and cosmic rays and  $Z$  decays are excluded. We compute  $M_T \equiv \sqrt{2p_T^\ell p_T^\nu [1 - \cos(\phi_{\ell\nu})]}$ , where  $\phi_{\ell\nu}$  is the azimuthal angle between  $\ell$  and  $\nu$ . Monte Carlo simulation is used to estimate the backgrounds, which are  $W \rightarrow \tau\nu \rightarrow \ell\nu\nu\nu$ ,  $Z \rightarrow \ell^+\ell^-$  (where one lepton is missed), and multijet events in which one jet is misidentified as a lepton and one is mismeasured to mimic  $\cancel{E}_T$ . Lepton energy scales and resolution are determined by comparing  $Z$  candidate  $M^{\ell\ell}$  spectra to LEP values of the  $Z$  mass and width. The  $M_T$  spectrum is predicted for several values of  $\Gamma_W$ . Data are normalized to the predicted number of events in the range  $100 < M_T < 200$  GeV. A fit to a likelihood function is used to extract  $\Gamma_W$ . The result is  $\Gamma_W = 2.04 \pm 0.11 \pm 0.09$  GeV, in good agreement with the Standard Model. Figures 31 and 32 show the  $M_T$  spectra in the  $e$  and  $\mu$  channels, respectively.

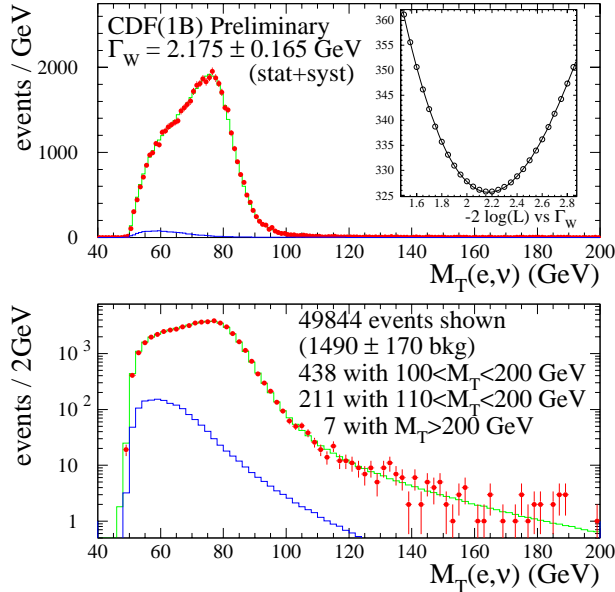


Figure 31: Transverse mass spectra (filled circles) for  $W \rightarrow e\nu$  data, with the best fit superimposed as a solid curve. The lower curve shows the sum of estimated backgrounds. The inset shows the 50-100 GeV region on a linear scale.



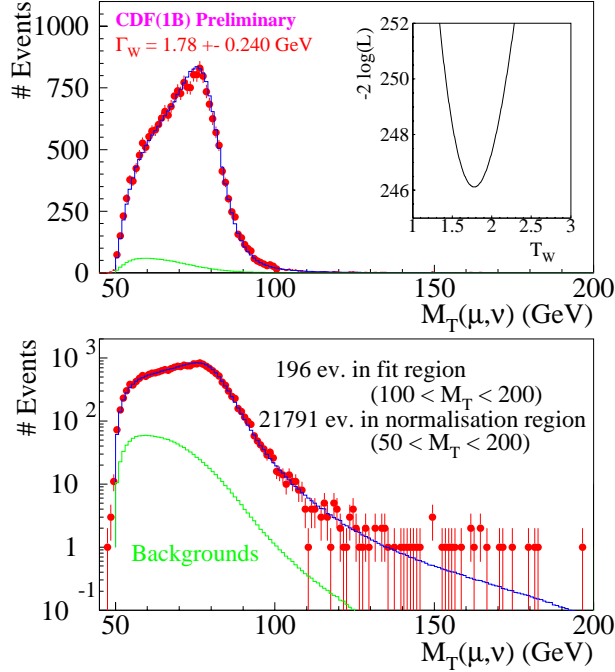


Figure 32: Transverse mass spectra (filled circles) for  $W \rightarrow \mu\nu$  data, with the best fit superimposed as a solid curve. The lower curve shows the sum of estimated backgrounds. The inset shows the 50-100 GeV region on a linear scale.

## References

- [1] F. Abe, *et al.*, Nucl. Instr. and Meth. A **271**, 387 (1988); D. Amidei, *et al.*, Nucl. Instr. and Meth. A **350**, 73 (1994); F. Abe, *et al.*, Phys. Rev. D **52**, 4784 (1995); P. Azzi, *et al.*, Nucl. Instr. and Meth. A **360**, 137 (1995).
- [2] F. Abe, *et al.*, Phys. Rev. D **61**, 032001 (2000).
- [3] T. Affolder, *et al.*, Phys. Rev. Lett. **84**, 1663 (2000).
- [4] T. Affolder, *et al.*, Phys. Rev. Lett. **85**, 2886 (2000).
- [5] T. Affolder, *et al.*, Phys. Rev. Lett. **84**, 2094 (2000).
- [6] T. Affolder, *et al.*, FERMILAB-PUB-99/330-E, 1999.
- [7] T. Affolder, *et al.*, Phys. Rev. Lett. **84**, 845 (2000).
- [8] J. Liu, Bulletin of the American Physical Society Centennial Meeting, Vol. 44, No. 1, Part 1, p. 405 (1999).
- [9] T. Affolder, *et al.*, Phys. Rev. Lett. **84**, 1110 (2000).
- [10] T. Affolder, *et al.*, Phys. Rev. Lett. **85**, 2062 (2000).
- [11] T. Affolder, *et al.*, Phys. Rev. Lett. **85**, 2056 (2000).
- [12] F. Abe, *et al.*, Phys. Rev. Lett. **84**, 5716 (2000).
- [13] T. Affolder, *et al.*, Phys. Rev. Lett. **84**, 835 (2000).
- [14] T. Affolder, *et al.*, Phys. Rev. Lett. **85**, 1378 (2000).

- [15] T. Affolder, *et al.*, Phys. Rev. Lett. **84**, 5704 (2000).
- [16] T. Affolder, *et al.*, Phys. Rev. D **62**, 012004 (2000).
- [17] T. Affolder, *et al.*, Phys. Rev. Lett. **84**, 216 (2000).
- [18] T. Affolder, *et al.*, FERMILAB-PUB-00/101-E, 2000.
- [19] T. Affolder, *et al.*, Phys. Rev. Lett. **85**, 3347 (2000).